Supporting Information

Core-Shell $[Cu_{45}(C_6H_{11}S)_{24}(P(PhF)_3)_4H_{19}]^{2+}$ Nanocluster: Synthesis, Structure and Catalytic Hydroboration

Hang Yu[a,‡] Jianmei Jia,[a,‡] Tao Yang,[a] Kai Chen,[a] Shan Jin,[a,*] Lin Xiong,[b,*] and Manzhou Zhu[a,*]

[a] Institutes of Physical Science and Information Technology, Key Laboratory of Structure and Functional Regulation of Hybrid Materials of Ministry of Education, Centre for Atomic Engineering of Advanced Materials, Department of Chemistry and Anhui Province Key Laboratory of Chemistry for Inorganic/Organic Hybrid Functionalized Materials, Anhui University, Hefei, Anhui 230601, PR China.

[b] School of Food and Chemical Engineering, Shaoyang University, Shaoyang 422000, PR China

E-mails: jinshan@ahu.edu.cn (S.J.); linxiong@hnsyu.edu.cn (L.X); zmz@ahu.edu.cn (M.Z.Z)

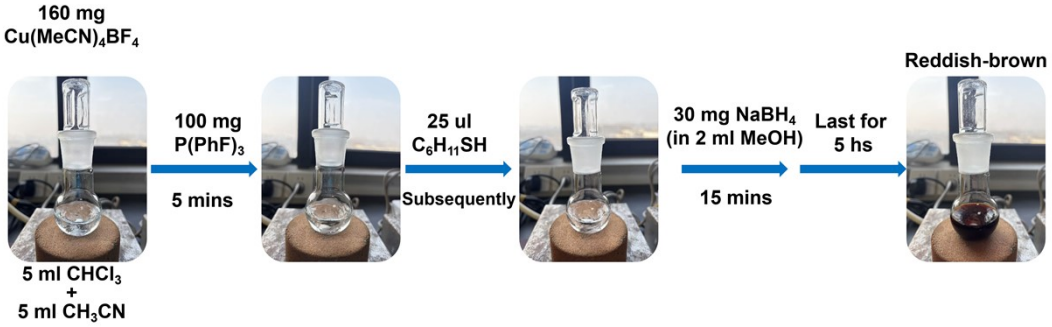

Figure S1. Digital photographs of the $[Cu_{45}(C_6H_{11}S)_{24}(P(PhF)_3)_4H_{19}]^{2+}$ synthesis process.

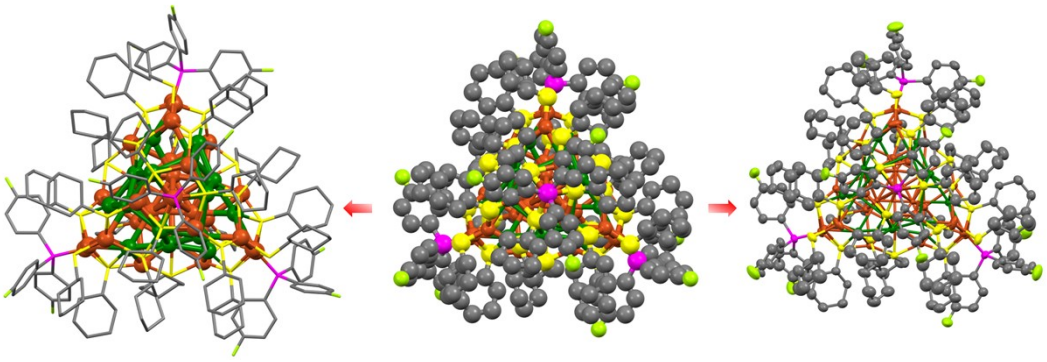

Figure S2. The overall structure and ORTEP drawing (50% probability) of $[Cu_{45}(C_6H_{11}S)_{24}(P(PhF)_3)_4H_{19}]^{2+}$.

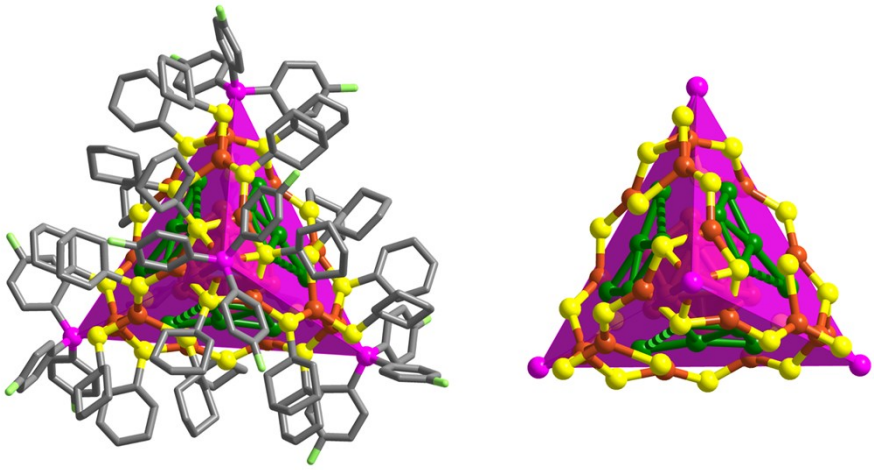

Figure S3. The overall structure exhibits a tetrahedral configuration.

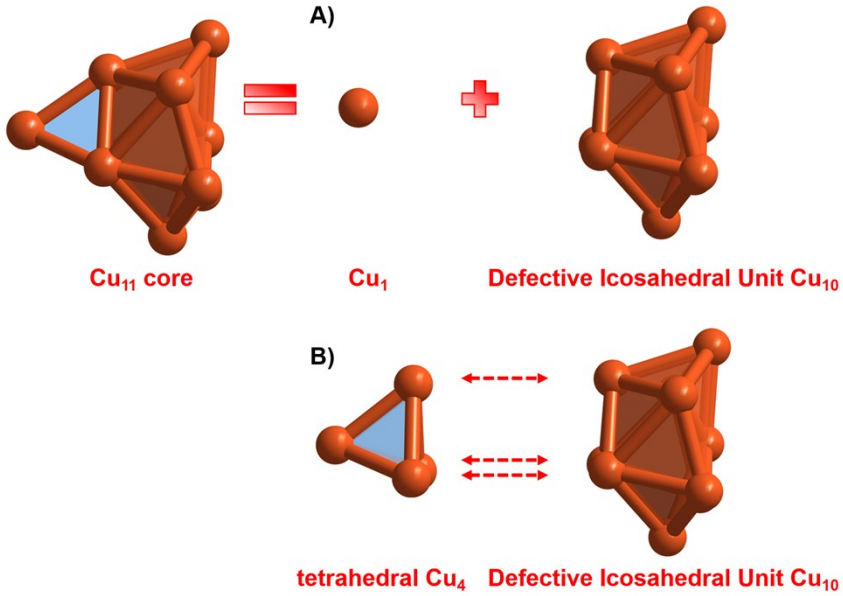

Figure S4. The structure of Cu_{11} core.

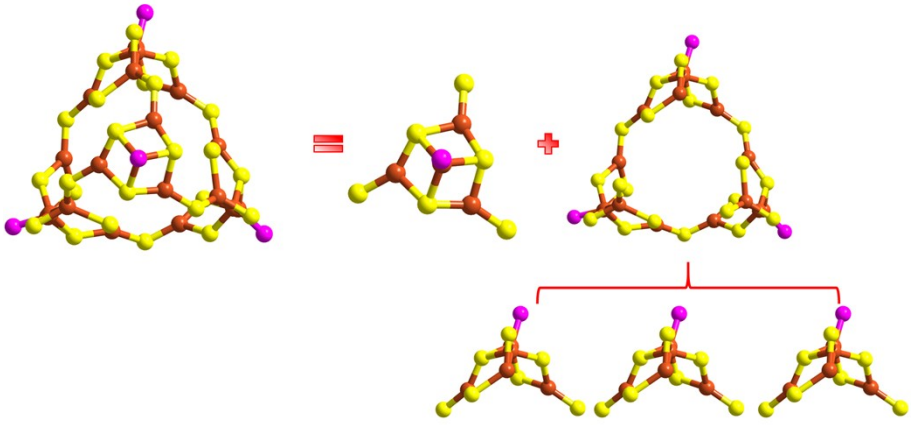

Figure S5. The structure of the cage-like metallic shell, $Cu_{19}(SR)_{24}(PR_3)_4$, can be viewed as a composite of $Cu_4(SR)_6(PR_3)$ and $Cu_{15}(SR)_{18}(PR_3)_3$, where the $Cu_{15}(SR)_{18}(PR_3)_3$ component itself is assembled from three simple $Cu_5(SR)_7(PR_3)$ staples.

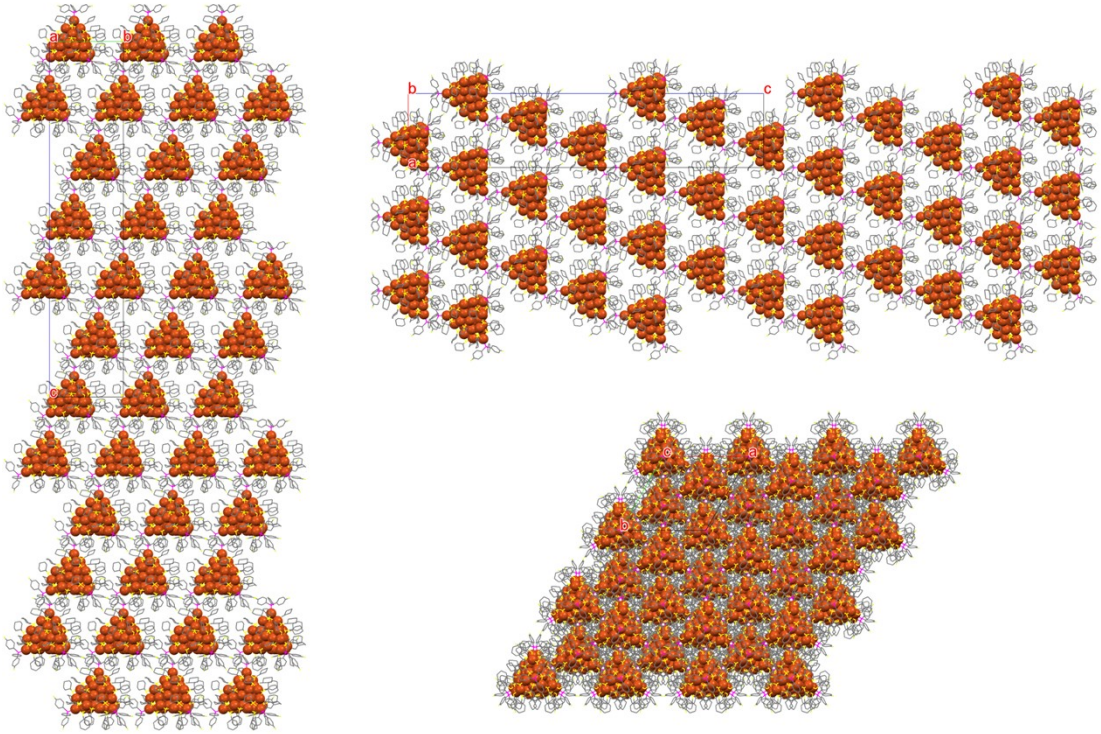

Figure S6. The packing mode of $[Cu_{45}(C_6H_{11}S)_{24}(P(PhF)_3)_4H_{19}]^{2+}$.

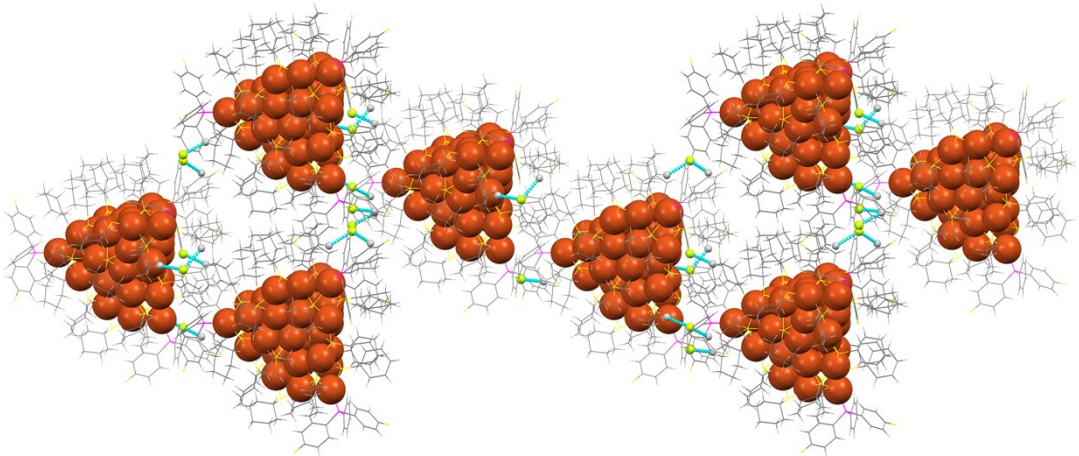

Figure S7. Intercluster C-H···F-C interactions in the unit cell of $[Cu_{45}(C_6H_{11}S)_{24}(P(PhF)_3)_4H_{19}]^{2+}$.

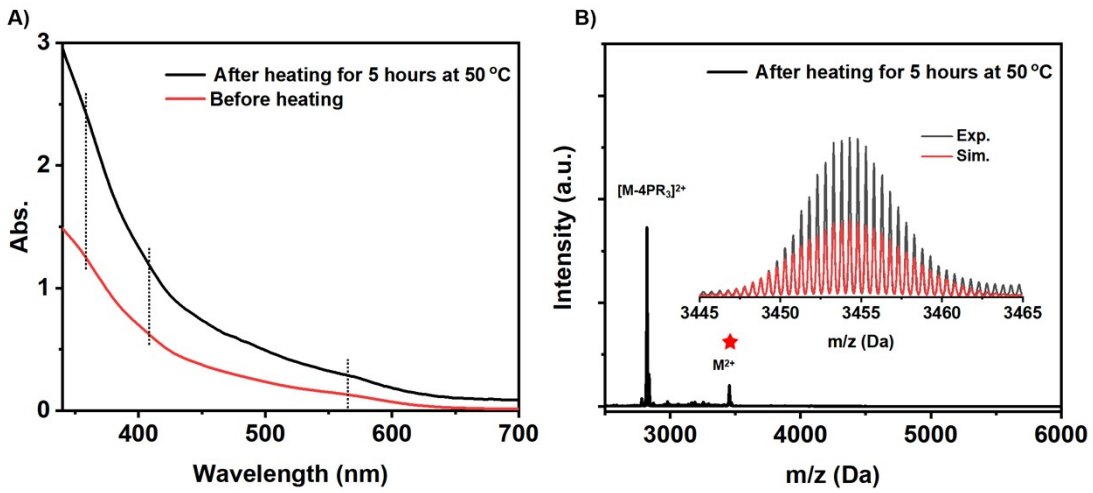

Figure S8. The optical absorption spectrum of $[Cu_{45}(C_6H_{11}S)_{24}(P(PhF)_3)_4H_{19}]^{2+}$ stored in a Schlenk tube was measured after heating for 5 hours at 50 °C and the corresponding ESI-MS data.

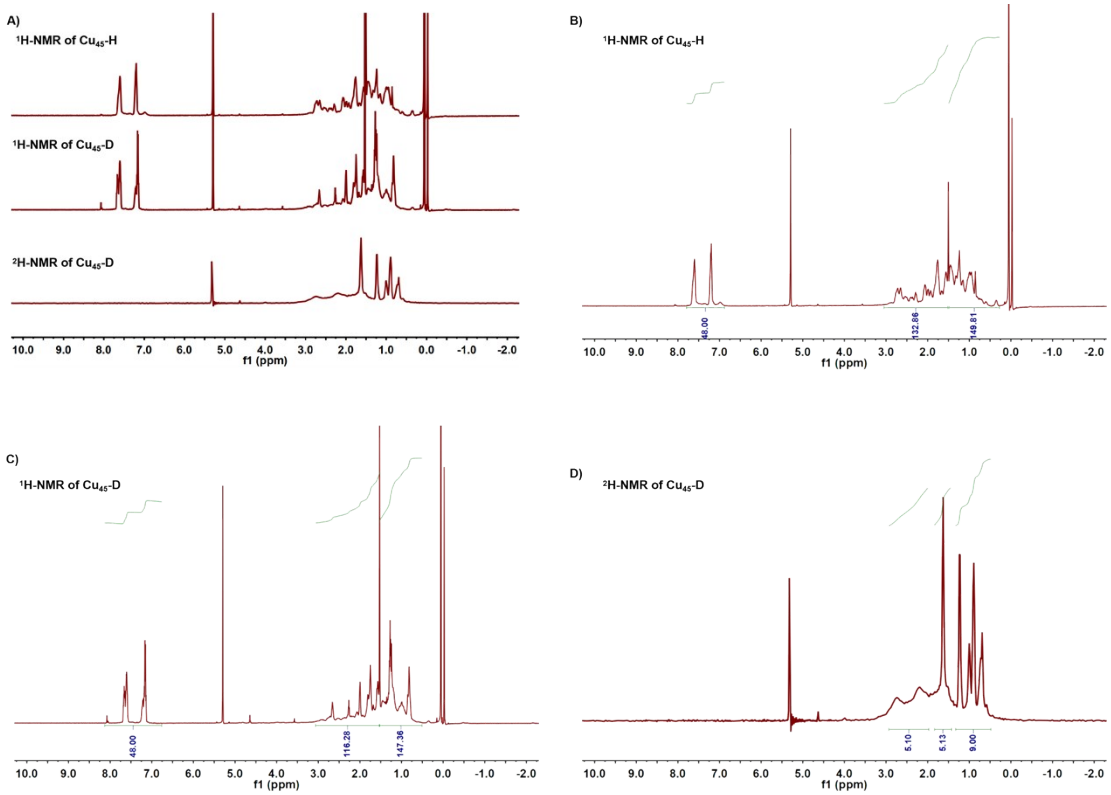

Figure S9. The NMR spectra of $[Cu_{45}(C_6H_{11}S)_{24}(P(PhF)_3)_4H_{19}]^{2+}$

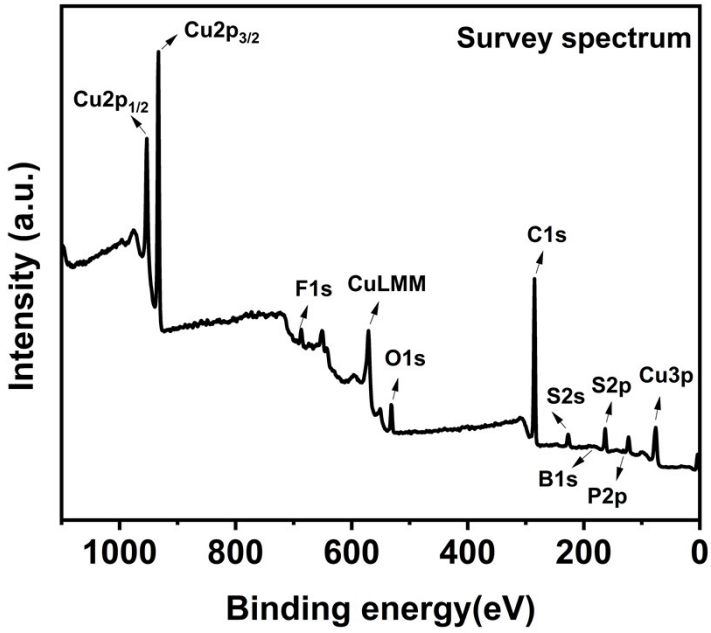

Figure S10. The XPS data of $[Cu_{45}(C_6H_{11}S)_{24}(P(PhF)_3)_4H_{19}]^{2+}$.

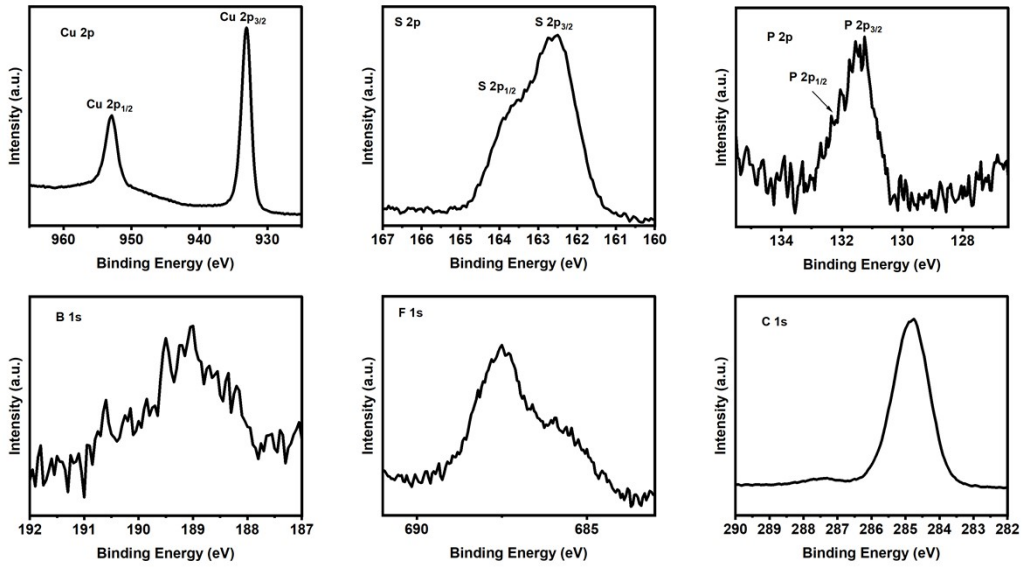

Figure S11. The detail XPS data of $[Cu_{45}(C_6H_{11}S)_{24}(P(PhF)_3)_4H_{19}]^{2+}$. The simultaneous appearance of the B and F signals indicates the presence of the BF_4^- counter-anion in the cluster complex. However, due to the limited crystal quality and the high symmetry of the crystal, this anion is often difficult to locate unambiguously within the unit cell.

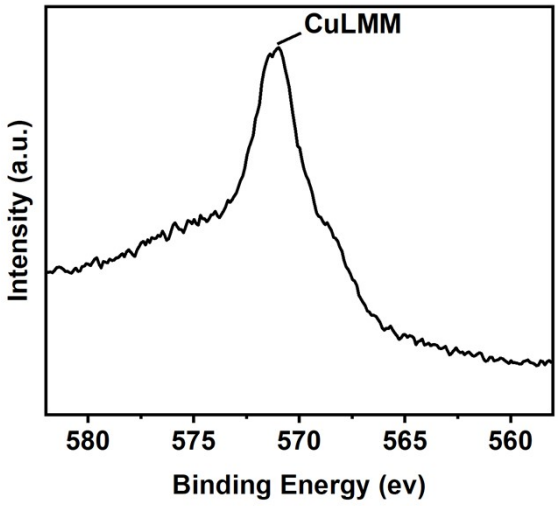

Figure S12. The Cu LMM auger spectrum of $[Cu_{45}(C_6H_{11}S)_{24}(P(PhF)_3)_4H_{19}]^{2+}$.

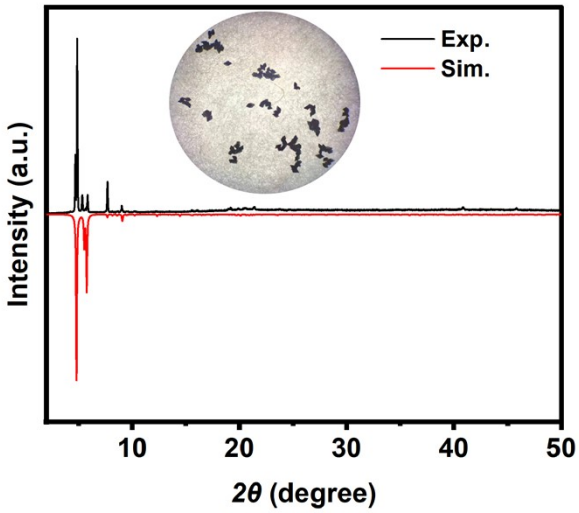

Figure S13. The PXRD spectra of $[Cu_{45}(C_6H_{11}S)_{24}(P(PhF)_3)_4H_{19}]^{2+}$.

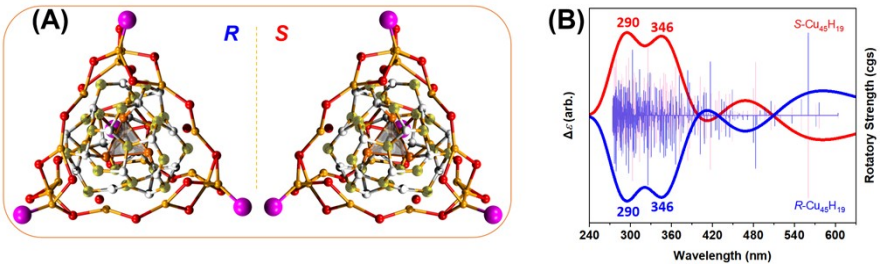

Figure S14. (A) Absolute configurations of two optically active **$Cu_{45}H_{19}$** clusters and (B) ECD spectra.

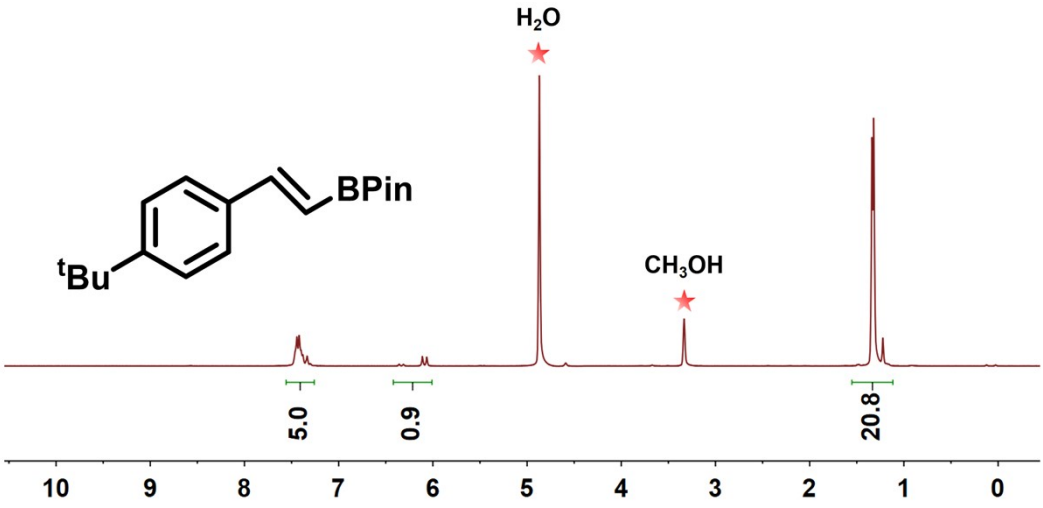

Figure S15. The ^{1}HNMR spectra of (E)-2-(4-(tert-butyl)styryl)-4,4,5,5-tetramethyl-1,3,2-dioxaborolane in CD_3OD solvent.

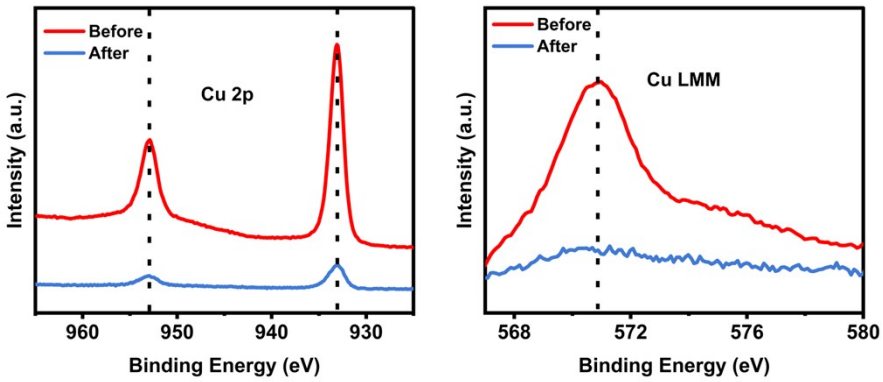

Figure S16. Comparison of the Cu 2p and Cu LMM spectra of catalyst **Cu_{45}** before and after reaction. The results show that the Cu 2p peaks and the Cu LMM features in the XPS spectra remain essentially unchanged, indicating that the surface clusters remain stable after the catalytic reaction.

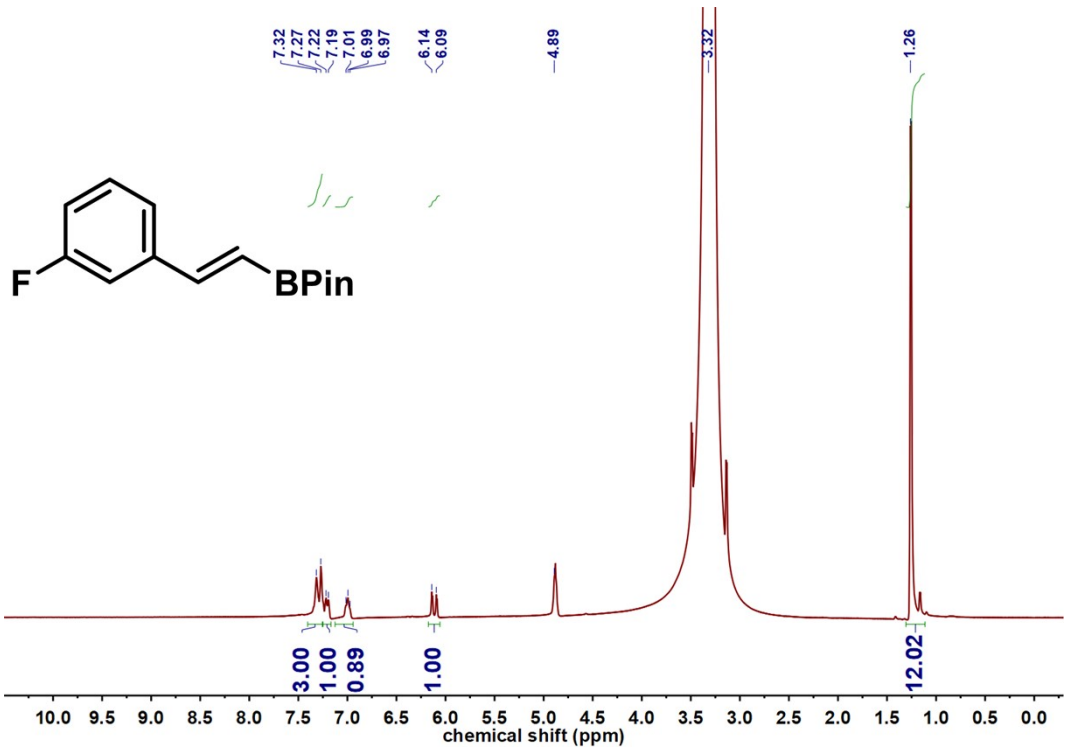

Figure S17. The ^{1}HNMR spectra of (E)-2-(3-fluorostyryl)-4,4,5,5-tetramethyl-1,3,2-dioxaborolane purification by silica gel column chromatography, eluent: PE/EtOAc = 4:1. Yield: 87.9%. ^{1}HNMR (600 MHz, CD_3OD), δ 7.29 (d, J = 16.3 Hz, 3H), 7.20 (d, J = 10.1 Hz, 1H), 6.99 (s, 1H), 6.12 (d, J = 18.4 Hz, 1H), 1.26 (s, 12H).

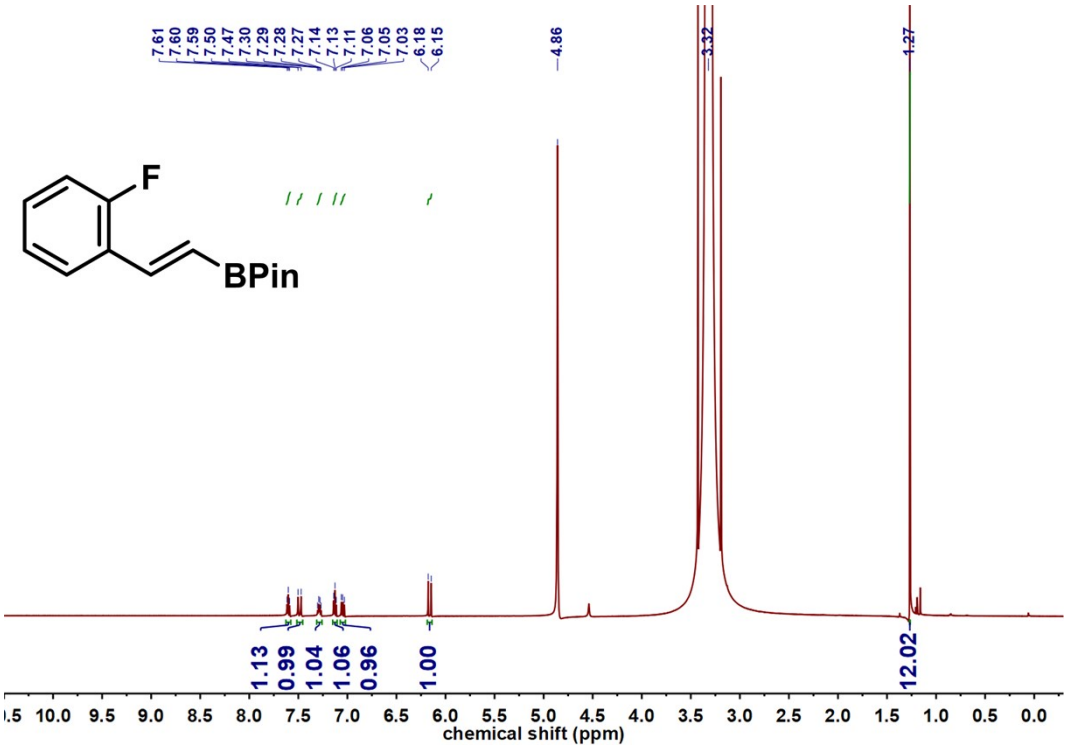

Figure S18. The ^{1}HNMR spectra of (E)-2-(2-fluorostyryl)-4,4,5,5-tetramethyl-1,3,2-dioxaborolane purification by silica gel column chromatography, eluent: PE/EtOAc = 4:1. Yield: 83.5%. ^{1}HNMR (600 MHz, CD_3OD), δ 7.13 (s, 1H), 6.16 (d, J = 18.6 Hz, 1H), 1.27 (s, 12H), 7.61 (d, J = 7.7 Hz, 1H), 7.49 (d, J = 18.6 Hz, 1H), 7.29 (q, J = 7.0 Hz, 1H), 7.05 (dd, J = 11.0, 8.2 Hz, 1H).

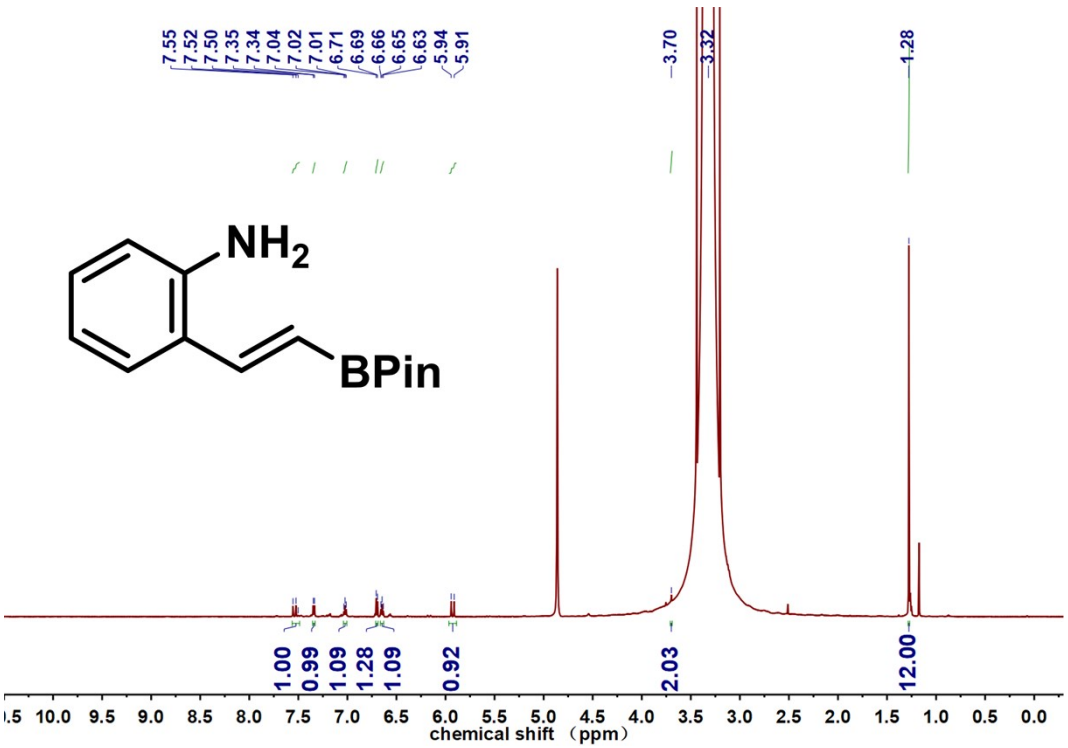

Figure S19. The [1]HNMR spectra of (E)-2-(2-(4,4,5,5-tetramethyl-1,3,2-dioxaborolan-2-yl)vinyl)aniline purification by silica gel column chromatography, eluent: PE/EtOAc = 4:1. Yield: 85.4%. 1HNMR (600 MHz, CD_3OD), δ 7.54 (d, J = 18.2 Hz, 1H), 7.34 (d, J = 7.8 Hz, 1H), 7.02 (t, J = 7.2 Hz, 1H), 6.70 (d, J = 7.9 Hz, 1H), 6.65 (t, J = 7.4 Hz, 1H), 5.93 (d, J = 18.2 Hz, 1H), 3.70 (s, 2H), 1.28 (s, 12H).

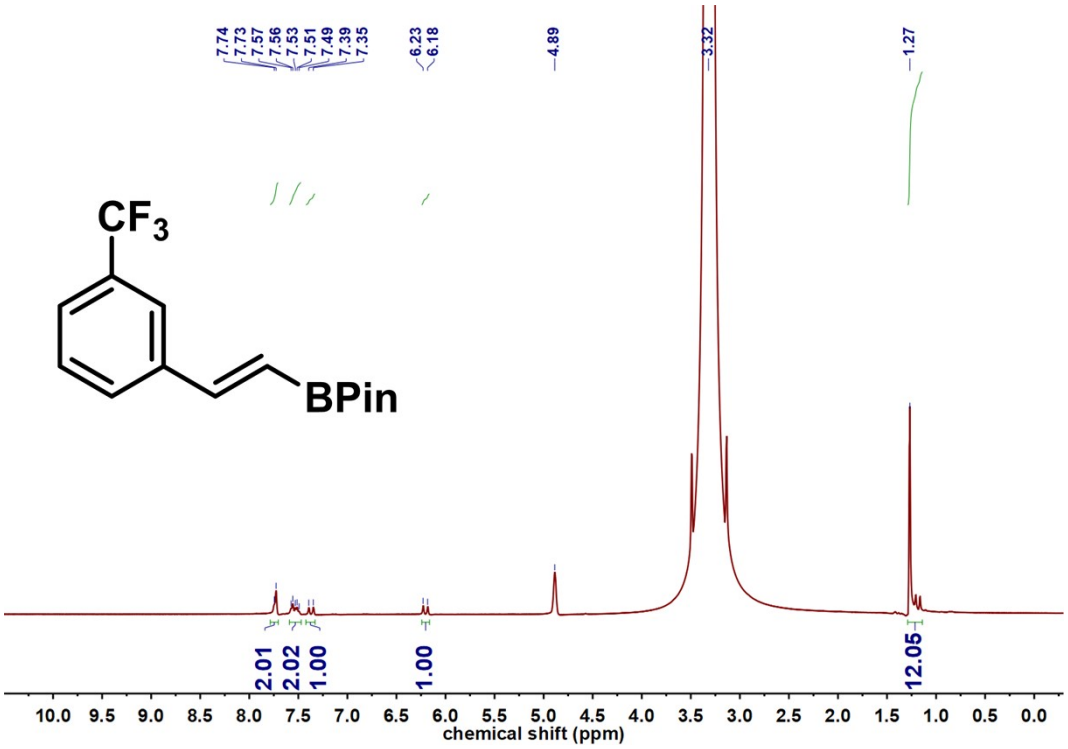

Figure S20. The [1]HNMR spectra of (E)-2-(4-(trifluoromethyl)styryl)-4,4,5,5-tetramethyl-1,3,2-dioxaborolane Purification by silica gel column chromatography, eluent: PE/EtOAc = 4:1. Yield: 86%.[1]HNMR (600 MHz, CD_3OD), δ 7.73 (d, J = 6.7 Hz, 2H), 7.53 (dt, J = 15.5, 7.4 Hz, 2H), 7.37

(d, J = 18.4 Hz, 1H), 6.21 (d, J = 18.4 Hz, 1H), 1.27 (s, 12H).

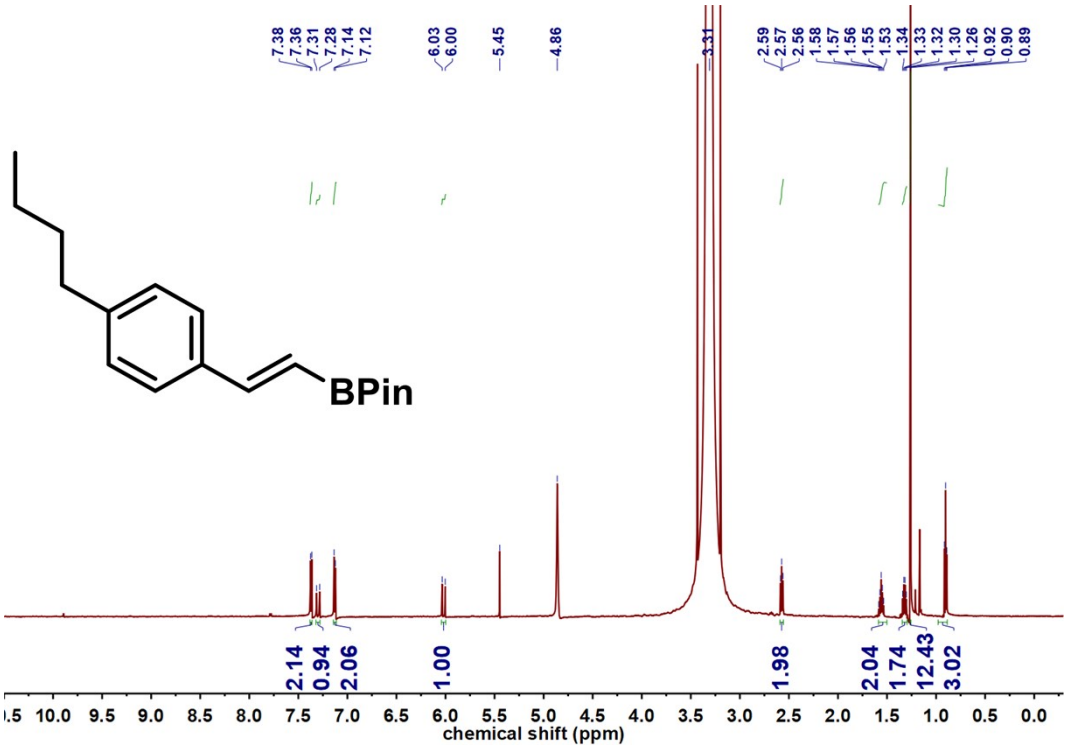

Figure S21. The ^{1}HNMR spectra of (E)-2-(4-Butylstyryl)-4,4,5,5-tetramethyl-1,3,2-dioxaborolane purification by silica gel column chromatography, eluent: PE/EtOAc = 4:1. Yield: 89.9%. 1H NMR (600 MHz, CD_3OD). δ 7.38 (d, J = 7.9 Hz, 2H), 7.31 (d, J = 18.4 Hz, 1H), 7.14 (d, J = 7.9 Hz, 2H), 6.03 (d, J = 18.4 Hz, 1H), 2.58 (t, J = 7.7 Hz, 2H), 1.57 (t, J = 7.7 Hz, 2H), 1.33 (d, J = 7.5 Hz, 2H), 1.27 (s, 12H), 0.91 (t, J = 7.4 Hz, 3H).

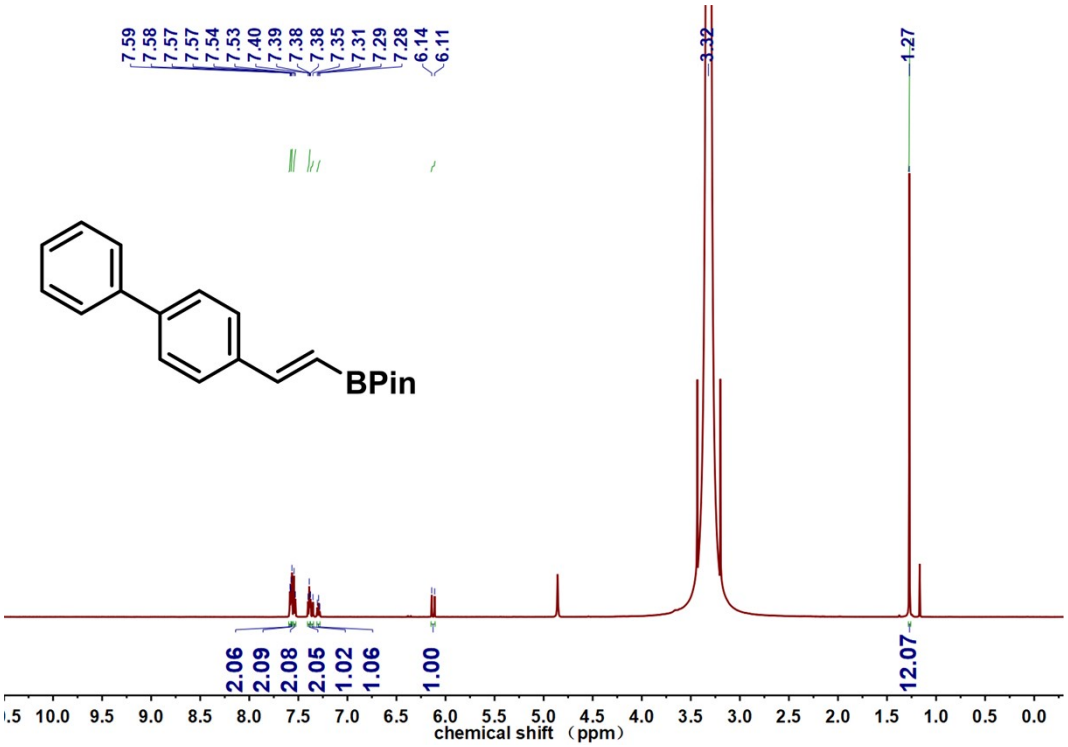

Figure S22. The ^{1}HNMR spectra of (E)-2-(2-([1,1'-biphenyl]-4-yl)vinyl)-4,4,5,5-tetramethyl-1,3,2-dioxaborolane purification by silica gel column chromatography, eluent: PE/EtOAc = 4:1.

Yield:96.1%. 1H NMR (600 MHz, CD_3OD). δ 7.60-7.56 (m, 2H), 7.54 (d, J = 8.2 Hz, 2H), 7.39 (t, J = 5.8 Hz, 2H), 7.35 (d, J = 14.5 Hz, 1H), 7.29 (t, J = 7.4 Hz, 1H), 6.13 (d, J = 18.3 Hz, 1H), 1.27 (s, 12H).

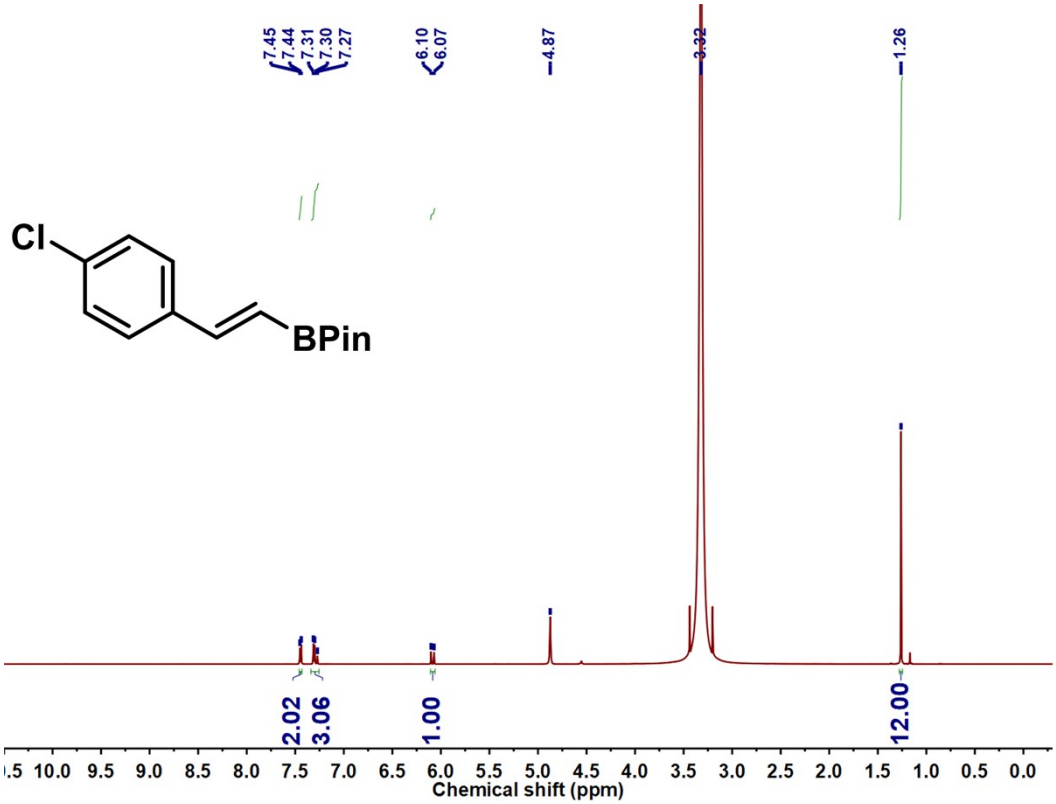

Figure S23. The [1]HNMR spectra of (E)-2-(4-chlorostyryl)-4,4,5,5-tetramethyl-1,3,2-dioxaborolane purification by silica gel column chromatography, eluent: PE/EtOAc = 4:1. Yield: 92.3%.[1]HNMR (600 MHz, CD_3OD), δ 7.47- 7.43 (m, 2H), 7.33 – 7.26 (m, 3H), 6.09 (d, J = 18.4 Hz, 1H), 1.26 (s, 12H).

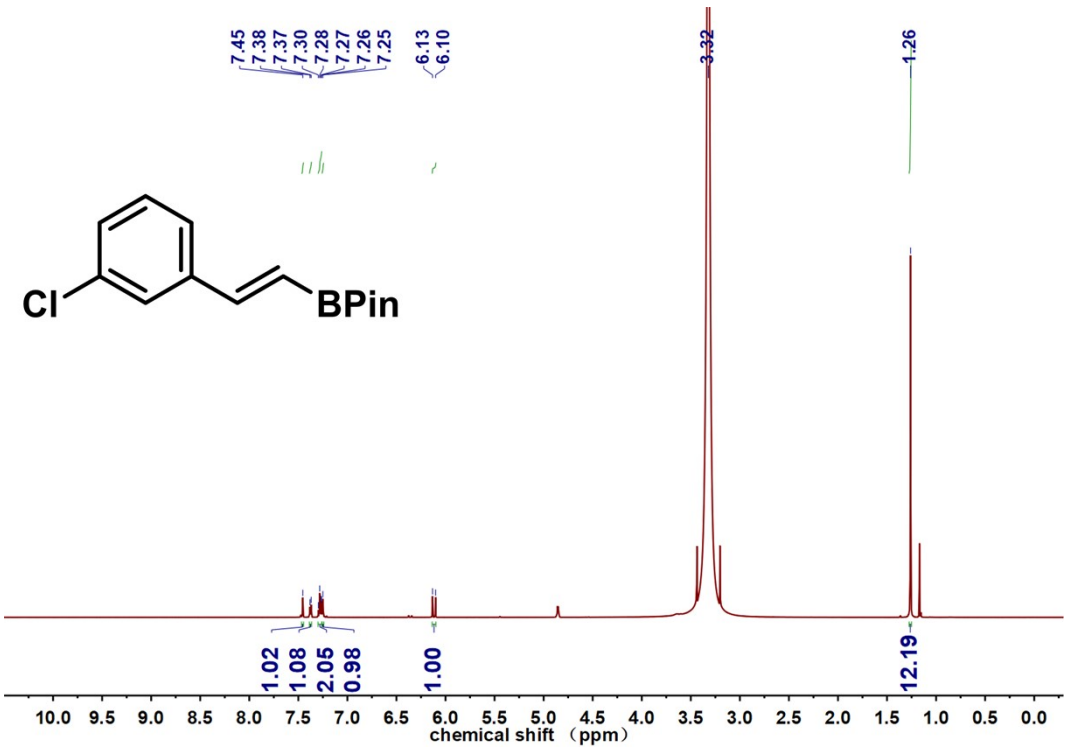

Figure S24. The [1]HNMR spectra of (E)-2-(3-chlorostyryl)-4,4,5,5-tetramethyl-1,3,2-dioxaborolane Purification by silica gel column chromatography, eluent: PE/EtOAc = 4:1. Yield:91.3%.[1]HNMR (600 MHz, CD_3OD), δ 7.46 (s, 1H), 7.38 (d, J = 7.3 Hz, 1H), 7.28 (t, J = 7.7 Hz, 2H), 7.25 (s, 1H), 6.12 (d, J = 18.4 Hz, 1H), 1.26 (s, 12H).

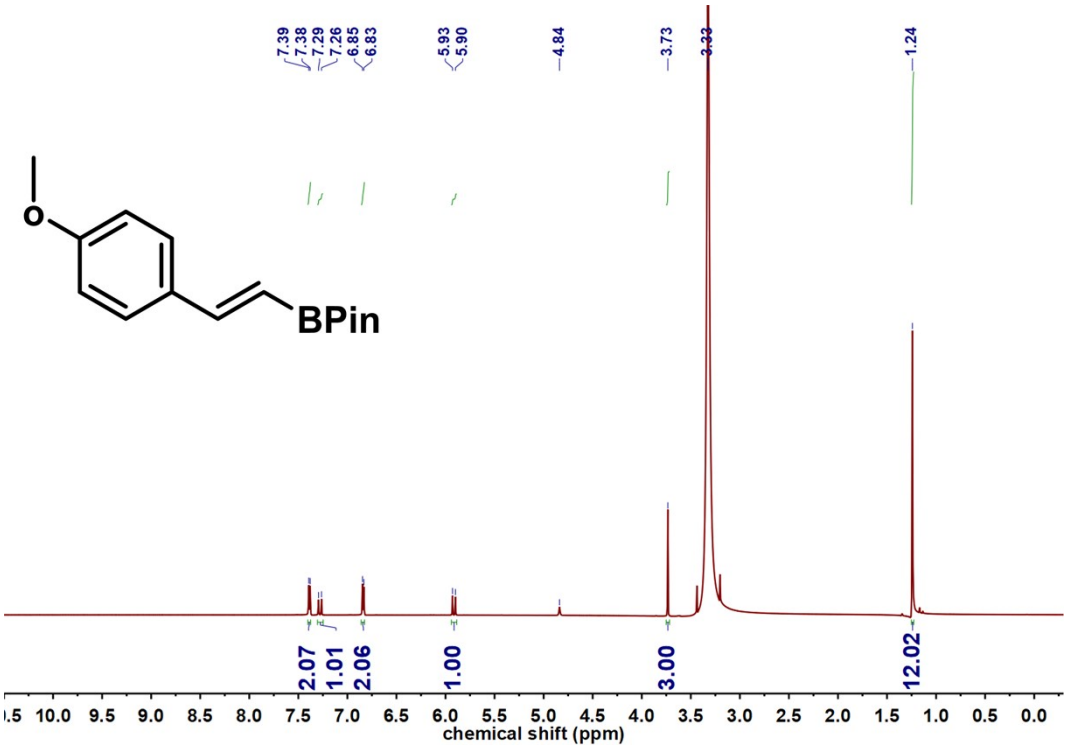

Figure S25. The [1]HNMR spectra of (E)-2-(4-Methoxystyryl)-4,4,5,5-tetramethyl-1,3,2-dioxaborolane purification by silica gel column chromatography, eluent: PE/EtOAc = 4:1. Yield: 94.8%. [1]HNMR (600 MHz, CD_3OD), δ 7.38 (d, J = 8.5 Hz, 2H), 7.29 (s, 1H), 6.83 (d, J = 8.5 Hz, 2H), 5.91 (d, J = 18.4 Hz, 1H), 3.73 (s, 3H), 1.24 (s, 12H).

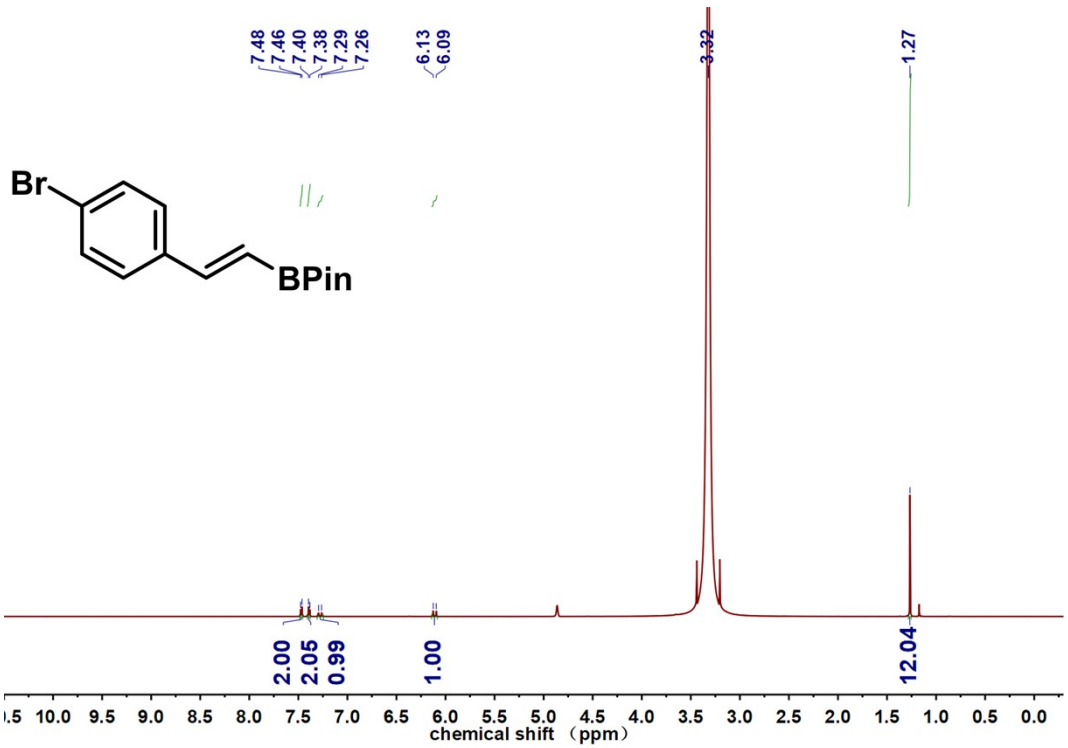

Figure S26. The ^{1}HNMR spectra of (E)-2-(4-bromostyryl)-4,4,5,5-tetramethyl-1,3,2-dioxaborolane purification by silica gel column chromatography, eluent: PE/EtOAc = 4:1. Yield: 85.3%. ^{1}HNMR (600 MHz, CD_3OD), δ 7.47 (d, J = 8.3 Hz, 2H), 7.39 (d, J = 8.3 Hz, 2H), 7.28 (d, J = 18.4 Hz, 1H), 6.11 (d, J = 18.4 Hz, 1H), 1.27 (s, 12H).

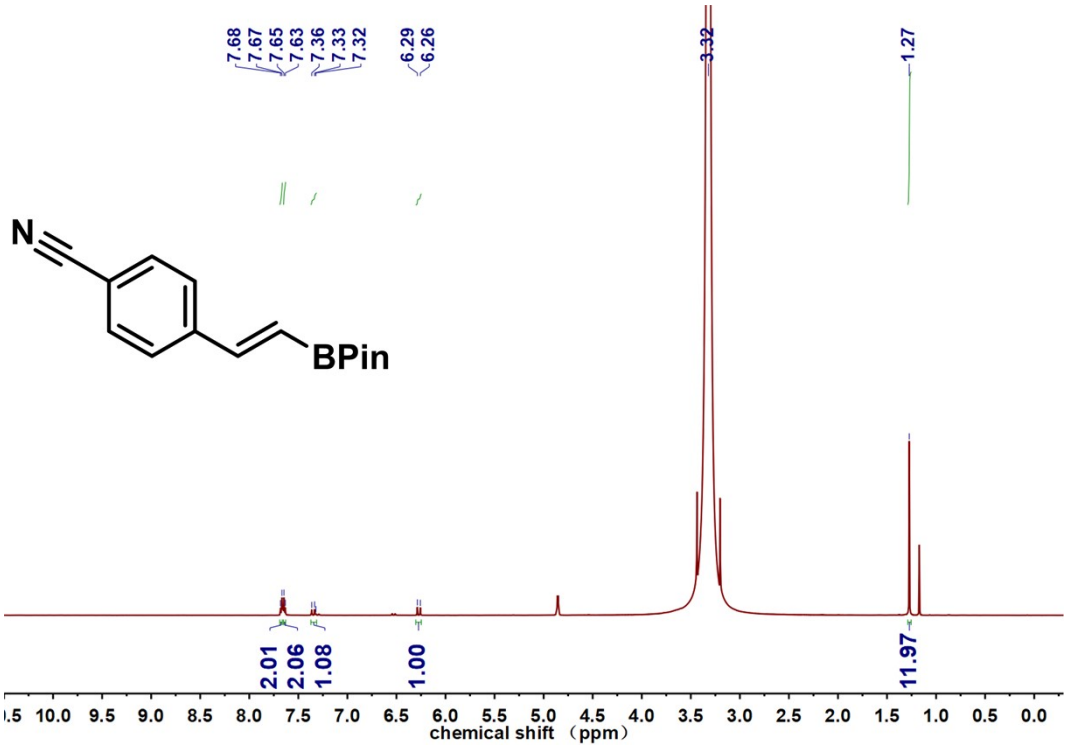

Figure S27. The ^{1}HNMR spectra of (E)-4-(2-(4,4,5,5-tetramethyl-1,3,2-dioxaborolan-2-yl)vinyl)benzonitrile purification by silica gel column chromatography, eluent: PE/EtOAc = 4:1. Yield: 83.8% 1H NMR (600 MHz, CD_3OD), δ 7.67 (d, J = 8.3 Hz, 2H), 7.64 (d, J = 8.2 Hz, 2H), 7.35 (d, J = 18.4 Hz, 1H), 6.27 (d, J = 18.4 Hz, 1H), 1.27 (s, 12H).

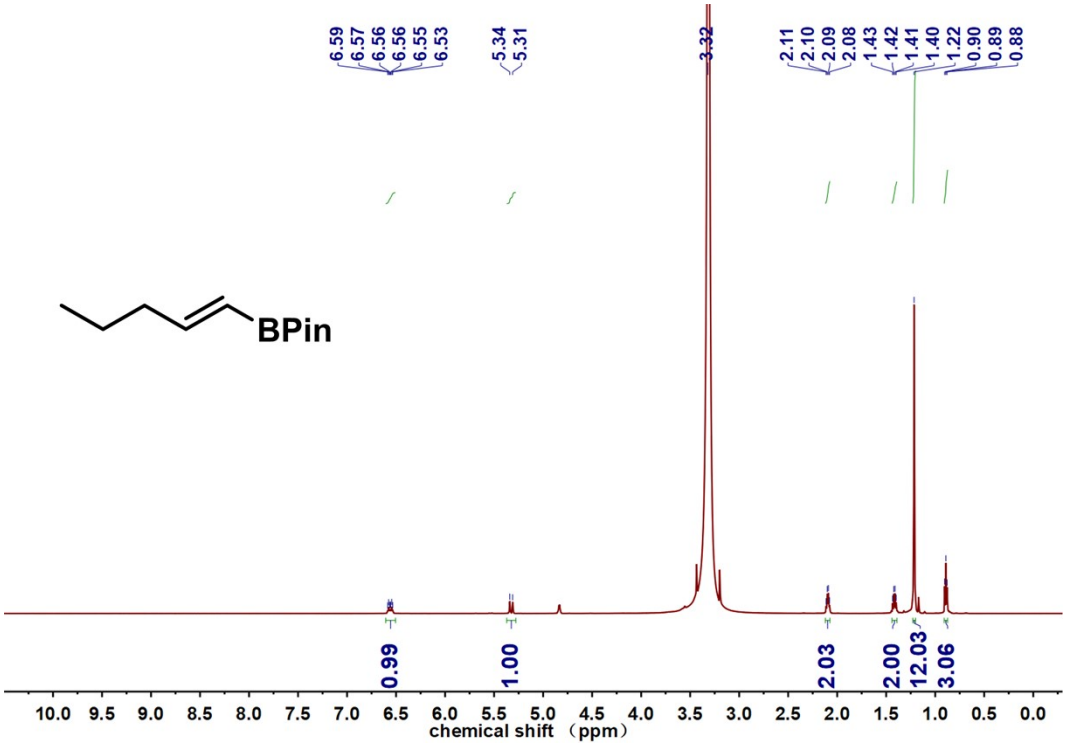

Figure S28. The [1]HNMR spectra of (E)-4,4,5,5-tetramethyl-2-(pent-1-en-1-yl)-1,3,2-dioxaborolane Purification by silica gel column chromatography, eluent: PE/EtOAc = 4:1. Yield: 83.2%.[1]HNMR (600 MHz, CD_3OD), δ 6.57 (dt, J = 18.0, 6.6 Hz, 1H), 5.33 (d, J = 17.9 Hz, 1H), 2.10 (q, J = 7.1 Hz, 2H), 1.42 (q, J = 7.4 Hz, 2H), 1.22 (s, 12H), 0.90 (t, J = 7.4 Hz, 3H).

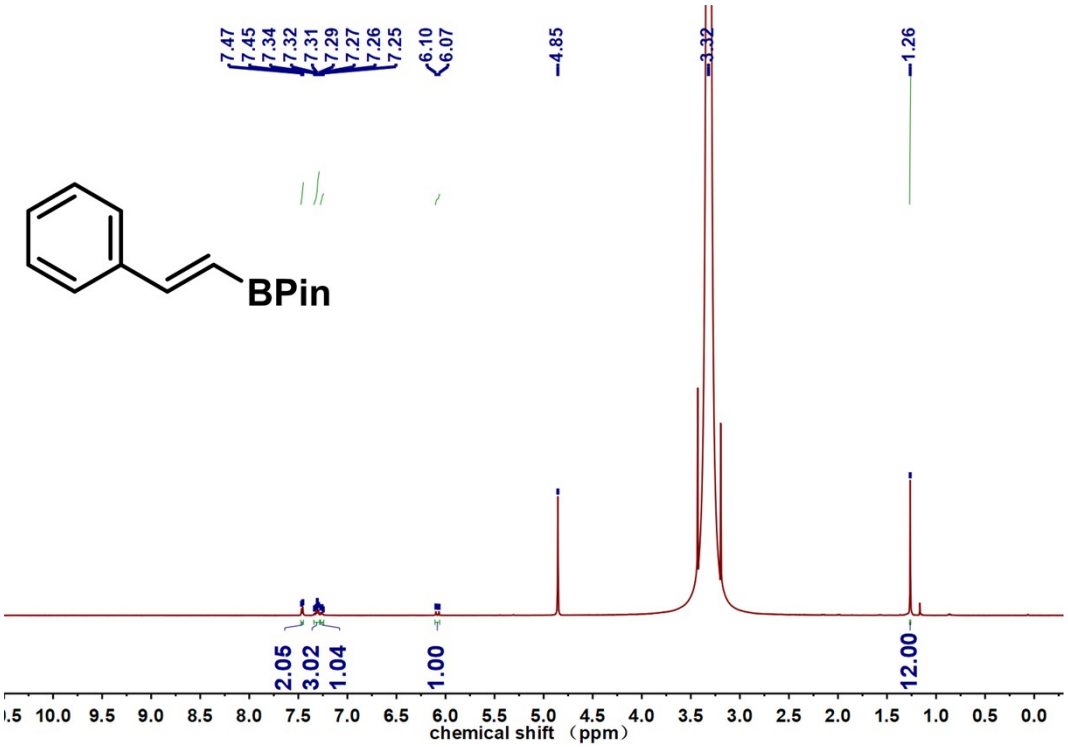

Figure S29. The [1]HNMR spectra of(E)-2-styryl-4,4,5,5-tetramethyl-1,3,2-dioxaborolane Purification by silica gel column chromatography, eluent: PE/EtOAc = 4:1. Yield: 95%. 1H NMR (600 MHz, CD_3OD), δ 7.47 (d, J = 7.4 Hz, 1H), 7.35 – 7.29 (m, 3H), 7.29 – 7.25 (m, 2H), 6.09 (d,

J = 18.4 Hz, 1H), 1.27 (s, 12H).

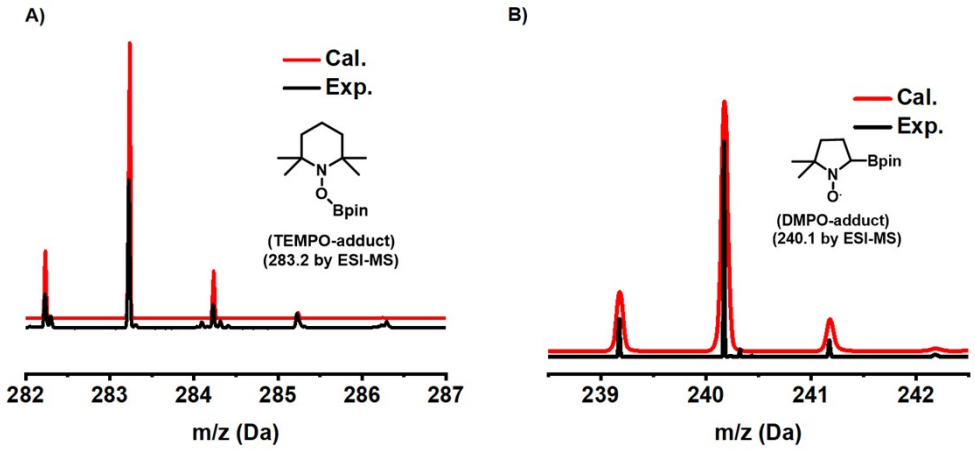

Figure S30. The ESI data of TEMPO-adducts (MW = 283.2) and DMPO-adducts (MW = 240.1).

Table S1.Crystal data and structure refinement for Cu_{45}-revised.

Identification code	Cu_{45}-revised
Empirical formula	$C_{216}H_{312}Cu_{45}F_{12}P_4S_{24}$
Formula weight	7104.17
Temperature/K	120(2)
Crystal system	trigonal
Space group	R3c
a/Å	22.9676(2)
b/Å	22.9676(2)
c/Å	95.6676(16)
α/°	90
β/°	90
γ/°	120
Volume/Å^3	43704.5(11)
Z	6
Radiation	CuKα (λ = 1.54186)
2θ range for data collection/°	7.698 to 139.414
Index ranges	$-27 \le h \le 26$, $-27 \le k \le 24$, $-116 \le l \le 63$
Reflections collected	168317

Independent reflections	13704 [R_{int} = 0.0594, R_{sigma} = 0.0301]
Data/restraints/parameters	13704/681/892
Goodness-of-fit on F^2	1.116
Final R indexes [I>=2σ (I)]	R_1 = 0.0999, wR_2 = 0.2404
Final R indexes [all data]	R_1 = 0.1035, wR_2 = 0.2450
Largest diff. peak/hole / e $Å^{-3}$	2.23/-1.06
Flack parameter	0.01(5)

Table S2. Attribution of the UV-Vis absorption peaks of **$Cu_{45}H_{19}$**.

Peak	**Excited state (Sn)**	**Wavelength (nm)**	**Oscillator Strength**	**Transition mode/contribution**
α	2	576.40	0.0125	H-2 → L 68.2%
				H-1 → L 17.9%
				H → L 7.8%
	3	571.88	0.03547	H-1 → L 63.0%
				H-2 → L 14.1%
				H-4 → L 9.9%
	4	560.51	0.0301	H-4 → L 58.3%
				H-3 → L 13.7%
				H-1 → L 9.4%
				H-5 → L 6.4%
				H-7 → L 5.2%
	5	550.55	0.01885	H-3 → L 55.3%
				H-4 → L 13.9%
				H-5 → L 11.5%
				H → L 11.0%
β	59	399.95	0.03887	H-15 → L+1 25.8%
				H-8 → L+2 21.4%
				H-10 → L+2 8.1%
				H-29 → L 5.1%
	62	396.88	0.02815	H-29 → L 17.7%
				H-27 → L 14.1%
				H-10 → L+2 11.8%
				H-8 → L+2 9.0%
				H-15 → L+1 8.5%
				H-25 → L 5.2%
				H-30 → L 5.2%
	63	394.6	0.02776	H-11 → L+2 26.9%
				H-28 → L 17.9%
				H-14 → L+2 5.7%
	64	393.1	0.02167	H-12 → L+2 35.7%
				H-13 → L+2 19.4%

				H-10 → L+2 6.8%
	67	390.5	0.02457	H-16 → L+1 48.3%
				H-18 → L+1 11.6%
γ	116	351.73	0.03685	H-1 → L+5 21.2%
				H-14 → L+3 8.1%
				H-12 → L+3 6.7%
	118	349.15	0.03494	H-43 → L 13.3%
				H-42 → L 12.2%
				H-23 → L+2 6.7%
				H-2 → L+5 6.3%
	124	346.13	0.0352	H-3 → L+5 23.1%
				H-41 → L 11.5%
				H-16 → L+3 6.9%